Temperature-dependent combinatorial level densities with the D1M Gogny force

S. Hilaire* and M. Girod
CEA, DAM, DIF, F-91297 Arpajon, France

S. Goriely
Institut d'Astronomie et d'Astrophysique, CP-226, Université Libre de Bruxelles, 1050 Brussels, Belgium

A. J. Koning
Nuclear Research and Consultancy Group, P.O. Box 25, NL-1755 ZG Petten, The Netherlands
(Received 16 May 2012; published 20 December 2012)

The combinatorial model of nuclear level densities has now reached a level of accuracy comparable to that of the best global analytical expressions without suffering from the limits imposed by the statistical hypothesis on which the latter expressions rely. In particular, it provides naturally, non-Gaussian spin distribution as well as nonequipartition of parities which are known to have a significant impact on cross section predictions at low energies. Our previous global model [S. Goriely, S. Hilaire, and A. J. Koning, Phys. Rev. C **78**, 064307 (2008)] suffered from deficiencies, in particular in the way the collective effects—both vibrational and rotational—were treated. We have recently improved the level density calculations using simultaneously the single-particle levels and collective properties predicted by a newly derived Gogny interaction [S. Goriely, S. Hilaire, M. Girod, and S. Péru, Phys. Rev. Lett. **102**, 242501 (2009)], therefore enabling a microscopic description of energy-dependent shell, pairing, and deformation effects. In addition, for deformed nuclei, the transition to sphericity is coherently taken into account on the basis of a temperature-dependent Hartree-Fock calculation which provides at each temperature the structure properties needed to build the level densities. This new method is described and shown to give reasonable results with respect to available experimental data.

DOI: 10.1103/PhysRevC.86.064317 PACS number(s): 21.10.Ma, 21.60.Jz, 21.10.Re

I. INTRODUCTION

The knowledge of nuclear level densities (NLDs) plays a key role in the evaluation of the nuclear data. It has been a field of research for years going back at least to 1936 with Bethe's pioneering work [1]. Level densities are required for modeling nuclear reactions as soon as the number of levels to which decay occurs is too large to allow for an individual description. With the development of new innovative facilities, as well as for astrophysical purposes, nuclear data far from the valley of stability are required. This challenges the nuclear reaction models. Indeed, so far, cross section predictions have mainly relied on more or less phenomenological approaches, depending on parameters adjusted to scarce experimental data or deduced from systematics. Such predictions are expected to be reliable for nuclei not too far from experimentally accessible regions, but are questionable when dealing with exotic nuclei. To face such difficulties, it is preferable to rely on as fundamental (microscopic) as possible methods based on physically sound models.

Global microscopic models of NLD have been developed over the last decades (see Ref. [2] and references therein), but they are almost never used for practical applications because of their lack of accuracy in reproducing experimental data (especially when considered globally on a large data set) or because they do not offer the same flexibility as do highly parametrized analytical expressions. We have therefore developed a combinatorial approach and demonstrated that it can clearly compete with the statistical ones in the global reproduction of experimental data [2,3]. This approach provides energy, spin, and parity dependence of NLD, and, at low energies, describes the nonstatistical limit which by definition cannot be described by the traditional statistical formulas. Such a nonstatistical behavior can have a significant impact on cross section predictions, particularly when calculating cross sections known to be sensitive to spin or parity distributions such as isomeric production cross sections [4] or capture cross sections. However, the combinatorial method described in Ref. [2] still offers room for improvement because of the phenomenological aspects of some ingredients it contains which could hamper its microscopic nature, and consequently its predictive power. For that reason, we have updated our method in order to reduce this amount of phenomenology.

Section II recalls the main features of the previously employed combinatorial method in order to shed light on the phenomenological components from which it still suffers. We describe in Sec. III the new features that have now been included, in particular the new nucleon-nucleon interaction together with the new structure properties that we use to construct our NLD, as well as the temperature-dependent treatment introduced to improve the description of the evolution of the nuclear deformation with increasing excitation energy. The obtained NLDs are compared with experimental data in Sec. IV. Conclusions and prospects are finally drawn in Sec. V.

*stephane.hilaire@cea.fr; http://www-phynu.cea.fr/

II. COMBINATORIAL MODEL OF NUCLEAR LEVEL DENSITIES

The combinatorial method has been extensively described in Refs. [2,3,5] and is only summarized here. It consists in using the single-particle level scheme obtained from the axially symmetric Hartree-Fock-Bogoliubov (HFB) method to construct incoherent particle-hole (ph) state densities $\omega_{\rm ph}(U, M, \pi)$ as functions of the excitation energy U, spin projection M, and parity π. Once these incoherent ph state densities are determined, collective effects are included. Vibrational effects are first accounted for using the boson partition function as introduced in Ref. [5] which includes quadrupole, octupole, as well as hexadecapole vibrational modes. This boson partition function depends only on the phonon's energies. In Ref. [5], only experimental data were used. To be able to provide NLDs for any nuclei, analytical systematics, adjusted on the tabulated data of Ref. [5], have been introduced in Ref. [3] for quadrupole and octupole vibrational modes and an extension for hexadecapole modes was also proposed in Ref. [2] to improve, in particular, the description of experimental s-wave mean spacings in the actinide region. Once the vibrational and incoherent ph state densities are obtained, they are folded in and yield the total state densities $\omega_{\rm tot}(U, M, \pi)$. To account for the damping of vibrational effects with increasing energies, we restrict the folding to the ph configurations having a total exciton number (i.e., the sum of the number of proton and neutron particles and proton and neutron holes) $N_{\rm ph} \leqslant 4$. This restriction stems from the fact that a vibrational state results from a coherent excitation of particles and holes, and that this coherence vanishes with increasing number of ph involved in the description. Level densities are then obtained by constructing rotational bands if the nucleus is deformed or using the classical expression relating state and level densities for a spherical nucleus. For spherical nuclei, the level density $\rho_{\rm s}(U, J, \pi)$ is obtained from the relation

$$\rho_{\rm s}(U, J, \pi) = \omega_{\rm tot}(U, M = J, \pi) - \omega_{\rm tot}(U, M = J + 1, \pi). \tag{1}$$

For deformed nuclei, within the axial symmetry hypothesis, the NLD reads

$$\rho_{\rm d}(U, J, \pi) = \frac{1}{2}\left[\sum_{K=-J, K\neq 0}^{J} \omega_{\rm tot}\left(U - E_{\rm rot}^{J,K}, K, \pi\right)\right] + \omega_{\rm tot}\left(U - E_{\rm rot}^{J,0}, 0, \pi\right) \times \left[\delta_{(J\ \text{even})}\delta_{(\pi=+)} + \delta_{(J\ \text{odd})}\,\delta_{(\pi=-)}\right]. \tag{2}$$

In the right-hand-side term of Eq. (2), the factor $1/2$ accounts for the fact that in mirror axially symmetric nuclei, the intrinsic states with spin projections $+K$ or $-K$ give rise to the same rotational levels. Moreover, in the second terms of the summation, the symbol $\delta_{(x)}$ (defined by $\delta_{(x)} = 1$ if x holds true and 0 otherwise) restricts the rotational bands built on intrinsic states with spin projection $K = 0$ and parity π to the levels sequences $0, 2, 4, \ldots$ for $\pi = +$ and $1, 3, 5, \ldots$ for $\pi = -$. Finally, the rotational energy is obtained with the well-known expression [6]

$$E_{\rm rot}^{J,K} = \frac{J(J+1) - K^2}{2\mathcal{J}_\perp}, \tag{3}$$

where $\mathcal{J}_\perp$ is the moment of inertia of a nucleus rotating around an axis perpendicular to the symmetry axis.

In Ref. [2], $\mathcal{J}_\perp$ was approximated by the rigid-body value $\mathcal{J}_\perp^{\rm rigid}$ which reads

$$\mathcal{J}_\perp^{\rm rigid} = \frac{2}{5} m R^2 \left(1 + \sqrt{\frac{5}{16\pi}}\beta_2\right),$$

for an ellipsoidal shape with axial quadrupole deformation parameter β_2.

Finally, because a deformed nucleus in its ground state becomes spherical with increasing excitation energies [7], this effect has to be taken into account. This was done in Refs. [2,3] introducing a phenomenological damping function $\mathcal{F}$ such that

$$\rho(U, J, \pi) = [1 - \mathcal{F}]\rho_s(U, J, \pi) + \mathcal{F}\rho_d(U, J, \pi). \tag{4}$$

The expression of $\mathcal{F}$ has evolved between Ref. [3] and Ref. [2], reflecting our lack of knowledge concerning this shape transition. In Ref. [3], $\mathcal{F}$ depended both on the excitation energy and the deformation of the nucleus, while in Ref. [2], it has been simplified to depend only on the nucleus deformation thus reducing the amount of phenomenology. The goal of this function was twofold: first, to describe smoothly the evolution from deformed to spherical shapes with increasing excitation energies, and, second, to smooth out the sharp transition appearing when one selects either Eqs. (1) or (2) (i.e., one decides if a nucleus is spherical or deformed) to determine level densities. Such a binary choice would have indeed given rise to sharp transitions within a given isotopic chain without any other physical justification than the arbitrary criterion used to decide when a nucleus is deformed or not.

To summarize, the collective features of the nuclei are among the major sources of uncertainty in the previously published methods. This concerns in particular the knowledge of vibrational level energies, for which the analytic expression of Refs. [2,3] is not satisfactory, as well as the evolution of the nucleus deformation with excitation energy. To improve the situation we have therefore modified our approach as we now describe.

III. IMPROVING THE DESCRIPTION OF COLLECTIVE EFFECTS

The starting point of our approach is a nucleon-nucleon effective interaction which provides within the framework of HFB calculation the single-particle level schemes upon which combinatorial level densities are determined. In our previous studies, the effective BSk14 Skyrme force [8] was used for this purpose, mainly because of its ability to reproduce nuclear binding energies with a relatively high accuracy. Indeed, the root mean square (rms) deviation of the HFB-14 mass model with respect to the 2149 measured masses [9] of nuclei with $Z, N \geqslant 8$ is 0.729 MeV. An alternative to this Skyrme interaction is the Gogny interaction, which has the advantage of also providing a fairly good description of low-energy

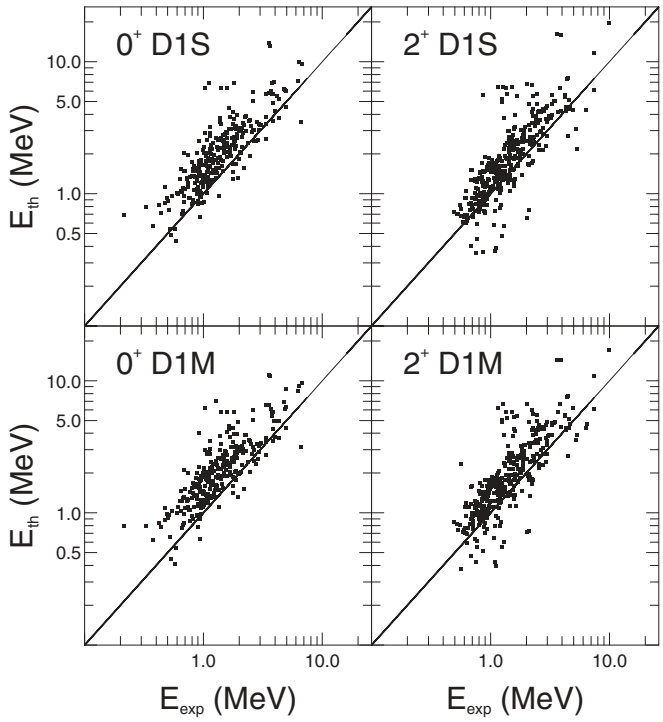

FIG. 1. Comparison between the energy of the experimental quadrupole vibrational 0^+ and 2^+ levels and those predicted using the approach described in Ref. [11] with the D1S and D1M interactions.

collective level properties [10,11]. The well-established D1S parametrization [12], however, turned out to be inappropriate for describing nuclear masses [13]. This situation has been recently improved [14] by modifying the Gogny force parameters in order to optimize the nuclear binding energy description without degrading the other qualities of the interaction, and in particular, the low-energy collective level properties. This feature is illustrated in Fig. 1 where the vibrational 0^+ and 2^+ levels obtained following the method described in Ref. [11] for both the D1S and D1M parametrizations are compared with experimental data of Ref. [5]. As can be observed, both interactions provide results of similar quality. Analyzing these results as in Ref. [10], we deduce that the predictions using the D1M interaction overestimate experimental data by a factor 1.28 for the 2^+ levels and 1.58 for the 0^+. Coming back to our combinatorial method, we can thus replace the analytical approximation for quadrupole vibrational energies introduced in our previous approaches by the D1M predictions. It is, however, worth mentioning that we apply globally the previously determined renormalization factors when using the D1M vibrational quadrupole energies in our boson partition function. Similar microscopic predictions would be required for octupole as well as for hexadecapole modes. Such predictions can be obtained using the quasiparticle random phase approximation [15,16], but this systematic study has not been performed yet.

Beyond the improved quadrupole vibrational energies, a new treatment has also been implemented to improve the description of the expected transition from deformed to spherical shape at increasing excitation energies. For this purpose, the temperature-dependent HFB approach is applied, following the method initially described in Ref. [17]. In Ref. [17], the average value of an observable $\mathcal{O}$ can be obtained from

$$\bar{\mathcal{O}} = \frac{\int \mathcal{O} \exp[-F(q)/T]dq}{\int \exp[-F(q)/T]dq}, \tag{5}$$

where the free energy F depends on the energy E, the temperature T, and the entropy S through the well-known relation $F(q) = E(q) - TS(q)$ and where q is the quadrupole deformation considered to be the most relevant degree of freedom to deal with deformation changes. Such a treatment would require quite extensive calculations since for each temperature a full potential energy surface has to be determined. Therefore, as a first step, a simpler approach has been adopted. It consists in determining the most probable deformation β_i by minimizing the free energy on the basis

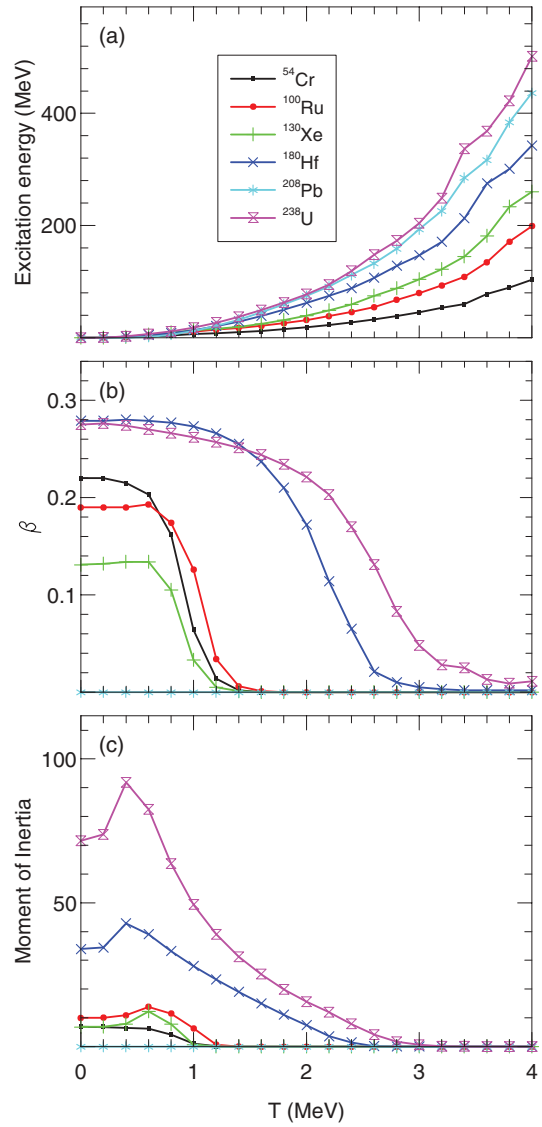

FIG. 2. (Color online) (a) Excitation energy as a function of the nuclear temperature T. (b) Quadrupole deformation parameter β as a function of T. (c) Moment of inertia as function of T.

of a temperature-dependent HFB calculation at a selected temperature T_i (corresponding to a given excitation energy U_i).

The corresponding evolution of the excitation energy U, quadrupole deformation β, and moment of inertia with increasing temperatures are illustrated in Fig. 2 for a set of nuclei covering a wide mass range and different initial deformations in their ground state. As expected, we recover the well-known $U \propto T^2$ relationship as well as the deformed to spherical shape transition.

To estimate the NLD at an excitation energy U_i and consequently at the corresponding deformation β_i, the same combinatorial method as described in Sec. II is used with the corresponding single-particle level scheme and pairing properties at the temperature T_i. It is also worth mentioning that this temperature-dependent approach provides microscopic moments of inertia which replace the rigid body value of Ref. [2] for the construction of the rotational bands of Eq. (3). The latter are also shown in Fig. 2 as functions of the temperature. Note that these moments of inertia $\mathcal{J}_\perp$ show nontrivial evolutions with increasing temperature. Indeed, they globally tend to increase at low T before decreasing at high temperatures. This feature stems from the competition between the deformation change and the gradual disappearance of pairing. More precisely, for low temperature, deformation changes are usually weak and the disappearance of pairing correlations thus dominate and explain the increase of the moment of inertia until the variations of $\mathcal{J}_\perp$ are essentially driven by deformation changes.

As illustrated in Fig. 3, the level densities are affected by the corresponding temperature-dependent nuclear input since they display discontinuities stemming from the disappearance (gradual or sudden) of the shell and pairing effects as well as from the fact that we use a finite set of temperatures. In principle the level density determined for a given temperature is only valid at the corresponding excitation energy. However, for practical reasons, we consider the NLD at T_i to be valid over the excitation energy interval $[U_i, U_{i+1}]$. In that case, to suppress the discontinuities, we consider that the level density

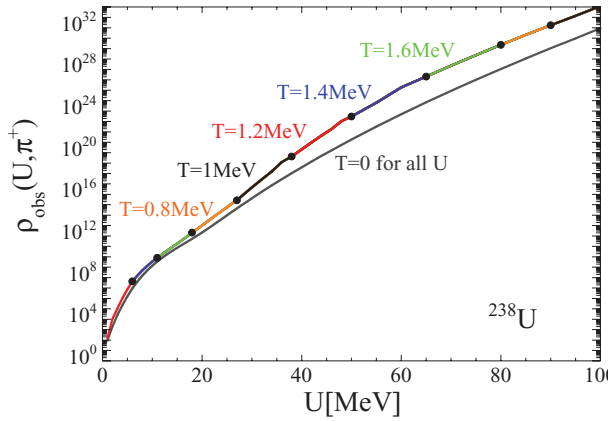

FIG. 4. (Color online) Total NLDs for positive parities of ^{238}U calculated for several temperatures connected smoothly thanks to the procedure described in the text. The reference points, i.e., those not affected by the smoothing procedure, are identified by circles. The level density obtained using the HFB ingredients determined with $T = 0$ at all excitation energies U is shown for comparison (lower grey curve).

calculated at T_i corresponds to the energy U_i, while the NLDs above U_i (up to U_{i+1}) have to be shifted in such a way as to recover the NLDs calculated at U_{i+1} on the basis of the HFB ingredients at T_{i+1}. With this treatment, the discontinuity shown in Fig. 3 in the T-dependent NLDs are smoothed out, as shown in Fig. 4. In most cases, the temperature-dependent NLD is found to be larger than that obtained with $T = 0$. For low excitation energies, this feature is mainly due to the vanishing of pairing correlations with increasing temperatures. For higher energies, in particular when pairing correlations disappear, the NLD enhancement stems from the increase of the density of the single-particle levels around the Fermi energy with increasing temperatures.

Last but not least, as we will see later, the damping function avoiding sharp transitions between the spherical and deformed

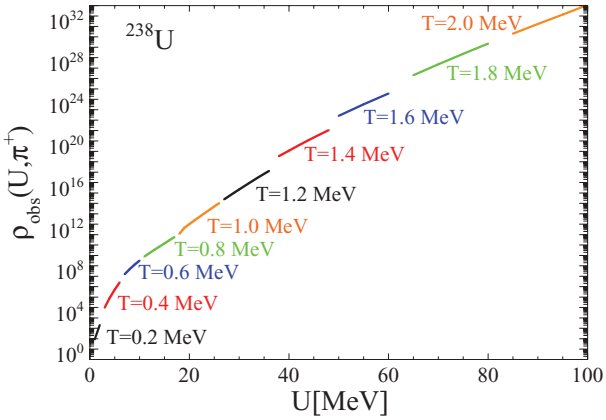

FIG. 3. (Color online) Total NLDs for positive parities of ^{238}U calculated for several temperatures. Each level density curve covers an energy interval which starts at the excitation energy corresponding to the chosen temperature.

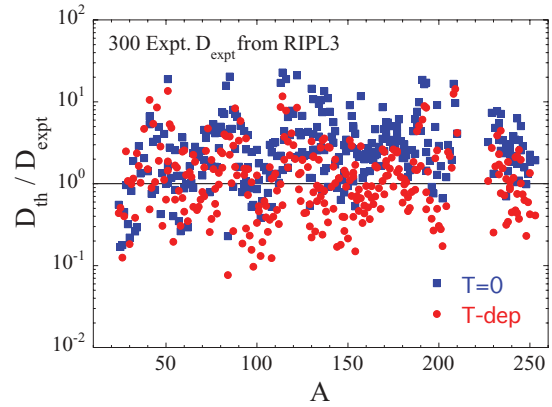

FIG. 5. (Color online) Ratio of HFB plus combinatorial (D_{th}) to the experimental (D_{expt}) s-wave neutron resonance spacings [20]. The temperature-dependent treatment is shown with circles and the $T = 0$ case with squares.

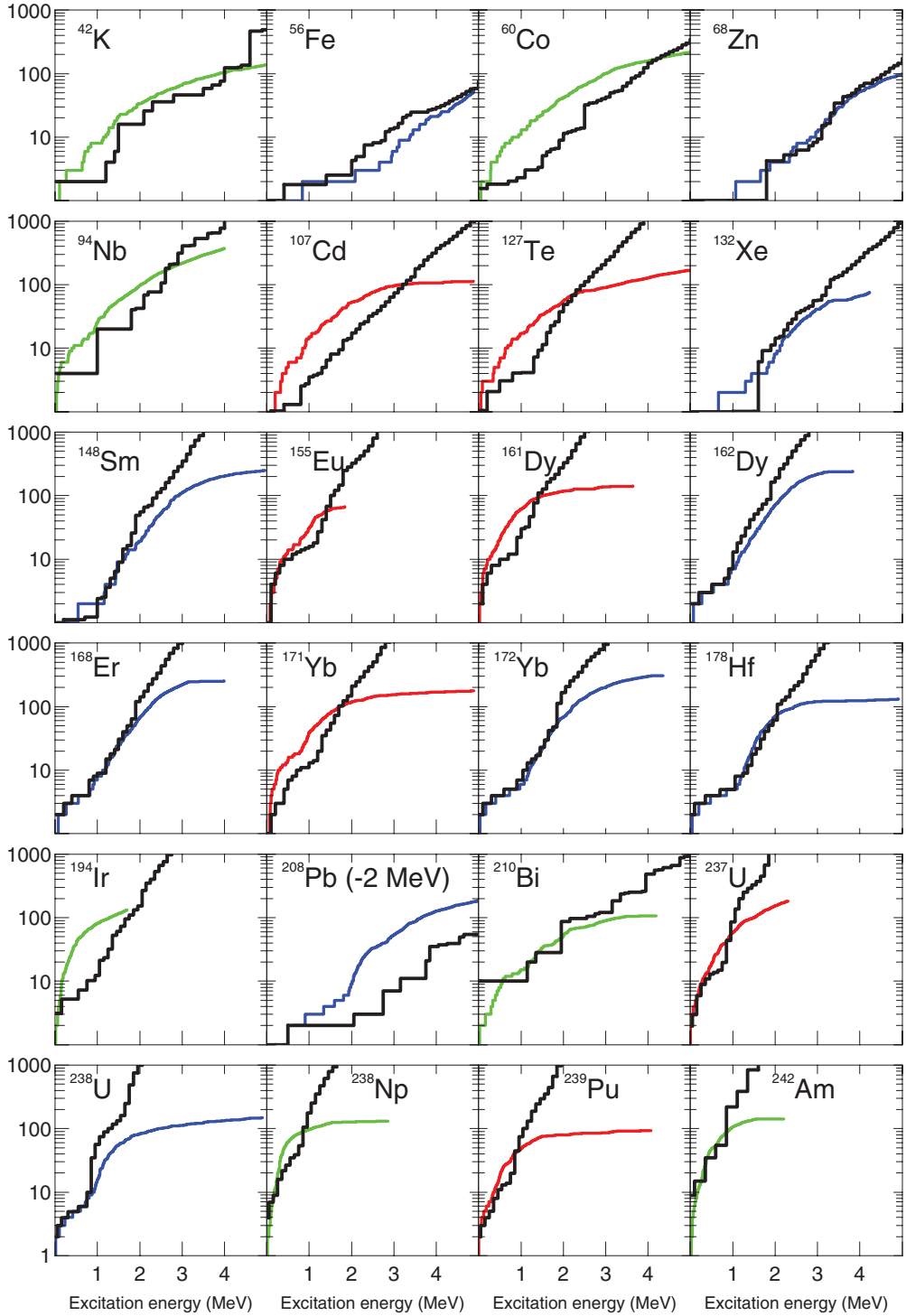

FIG. 6. (Color online) Comparison of the cumulative number of observed levels (colored lines) with the current combinatorial method (thick black line) as a function of the excitation energy for a sample of 24 nuclei. Experimental data for even-even, odd-A, and odd-odd nuclei are shown by the blue, red, and green lines, respectively. Only for ^{208}Pb, both curves have been shifted by 2 MeV, the energy range corresponding consequently to [2–7] MeV instead of [0–5] MeV.

level densities, as explained in Sec. II, has been modified. We now use an expression only depending on the quadrupole deformation parameter β_2 which reads

$$\mathcal{F} = 1 - [1 + e^{(\beta_2 - 0.19)/0.02}]^{-1}, \quad (6)$$

where the parameters have been adjusted in order to reproduce at best the s-wave mean spacings at the neutron separation energy. It is important to insist here on the fact that this damping function is used to suppress the discontinuities occurring between the spherical and deformed NLDs. This

is needed to avoid a sharp transition from one nucleus to the neighboring one when dealing with softly deformed nuclei, but not to describe shape evolutions with increasing excitation energies as was done in Ref. [3].

IV. RESULTS

The temperature-dependent NLD is found to be significantly different from that obtained at $T = 0$, as already illustrated in Fig. 4. The temperature effect may consequently have a non-negligible impact in particular on the s-wave spacings at S_n. To check that, we have applied the previously described method to all the nuclei for which experimental s-wave mean spacings D_0 exist. The results are displayed in Fig. 5 and compared with those obtained without any temperature dependence. The improvement obtained with the temperature-dependent method is quite clear. To measure the dispersion between theoretical and experimental D_0, we introduce as usual the $f_{\rm rms}$ factor defined as

$$f_{\rm rms} = \exp\left[\frac{1}{N_e}\sum_{i=1}^{N_e} \ln^2 \frac{D^i_{\rm th}}{D^i_{\rm expt}}\right]^{1/2}, \qquad (7)$$

where $D_{\rm th}$ ($D_{\rm expt}$) is the theoretical (experimental) resonance spacing and N_e is the number of nuclei in the compilation. While $f_{\rm rms} = 4$ without accounting for the temperature dependence (a value similar to the one obtained in Ref. [5] based on the D1S interaction), $f_{\rm rms} = 2.7$ with our new temperature-dependent treatment. It should, however, be mentioned that contrary to what has been done in Ref. [2], we have not included here any hexadecapole vibrational phonon. In the current situation, the only phenomenological ingredients are the octupole vibrational phonon energies, the number of phonons and ph configurations included in the vibrational-intrinsic state density folding procedure and the damping function [Eq. (6)]. The final $f_{\rm rms}$ is comparable to, even if slightly worse than, our 2008 compilation [2] ($f_{\rm rms} = 2.3$), the microscopic plus statistical formula ($f_{\rm rms} = 2.1$) of Ref. [18] as well as the value of $f_{\rm rms} = 1.8$ obtained with the phenomenological Back-Shifted Fermi Gas Model (BSFG) formula [19].

It is also important to check if the new level densities still behave correctly for low-lying discrete levels as in Ref. [2]. For this purpose, we compare in Fig. 6, for quite a large set of nuclei covering light and heavy as well as odd-odd, odd-A, and even-even species, the cumulated histograms of experimental low-energy levels with the theoretical predictions. As can be observed, an overall reasonable description of experiment is obtained.

When looking more carefully, a kind of systematic disagreement is, however, observed for odd-A as well as odd-odd nuclei. This feature has already been observed [21] and stems from the simple treatment of the coupling between particle-hole and vibrational states as currently implemented. Further investigations are, however, required to confirm this pattern. The description of a few nuclei, such as ^{60}Co, ^{107}Cd, ^{127}Te, or ^{194}Ir, clearly appears to be worse than that obtained with our previous model (see Fig. 6 of Ref. [2]). To understand this problem, we have adopted, as in Ref. [2], the rigid body value of the moment of inertia to construct the rotational bands and used either the damping function of Ref. [2] or the current one given by Eq. (6). The results are shown in Fig. 7. As can be seen, the good description of experimental data is recovered if one uses (i) a rigid body value for the moment of inertia and (ii) the damping function (thick line) of Ref. [2] while discrepancies are still clear when the current damping function is adopted (dotted line). If this sheds light on the difficulties related to the choice of the damping function, it also shows that the agreement observed in Ref. [2] stems from the use of a rigid body value for the moment of inertia, which is clearly not justified for low excitation energies where pairing correlations are known to strongly reduce the rotational

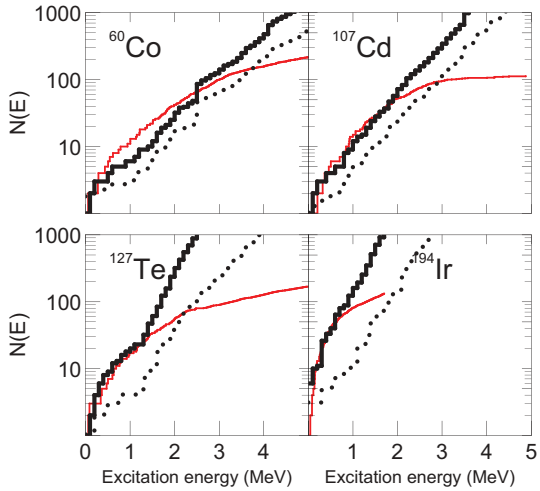

FIG. 7. (Color online) Same as Fig. 6, but for a sample of four nuclei for which a worse agreement with experiment (thin red line) than in Ref. [2] is observed. Theoretical predictions are obtained using the rigid body value for the moment of inertia and either the damping function of Ref. [2] (heavy black solid line) or the current damping function (black dotted line) given by Eq. (6). See text for more details.

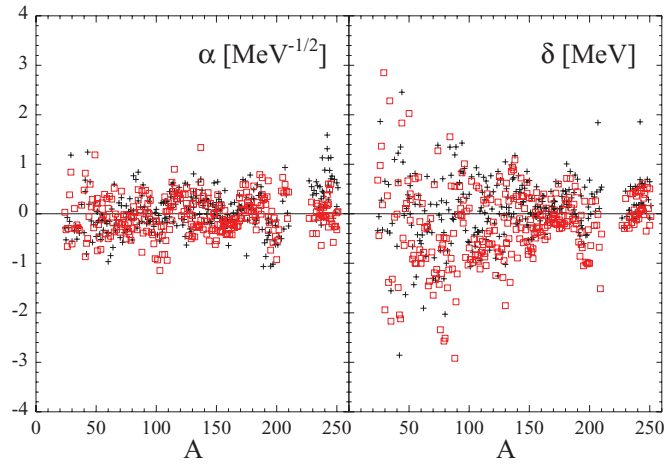

FIG. 8. (Color online) Current α and δ values (red squares) and those of Ref. [2] (black crosses) plotted as a function of the atomic mass. See text for more details.

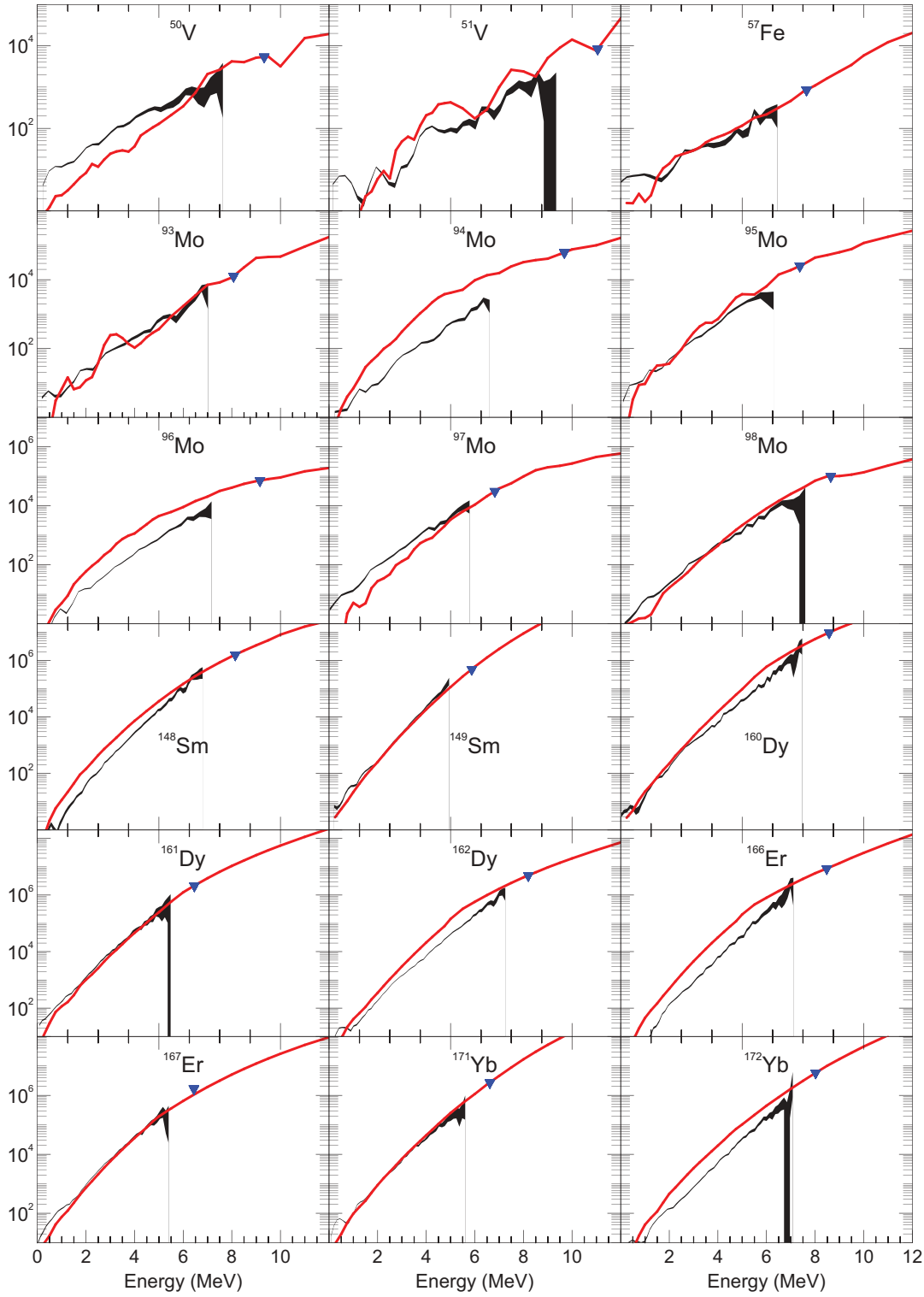

FIG. 9. (Color online) Comparison between the total NLDs determined by the Oslo group (grey areas) [23–25] and the HFB combinatorial predictions (thick lines). The full triangles correspond to the model-dependent normalization point derived by the Oslo group. See text for more details.

moment of inertia. This remark is furthermore confirmed by the better description of the low-energy experimental discrete levels in actinides (Fig. 6) with the current treatment of the moment of inertia. In other words, we believe that the good agreement obtained in Ref. [2] results from the compensation of the crude treatment of the coupling between particle-hole and vibrational states by too strong a moment of inertia.

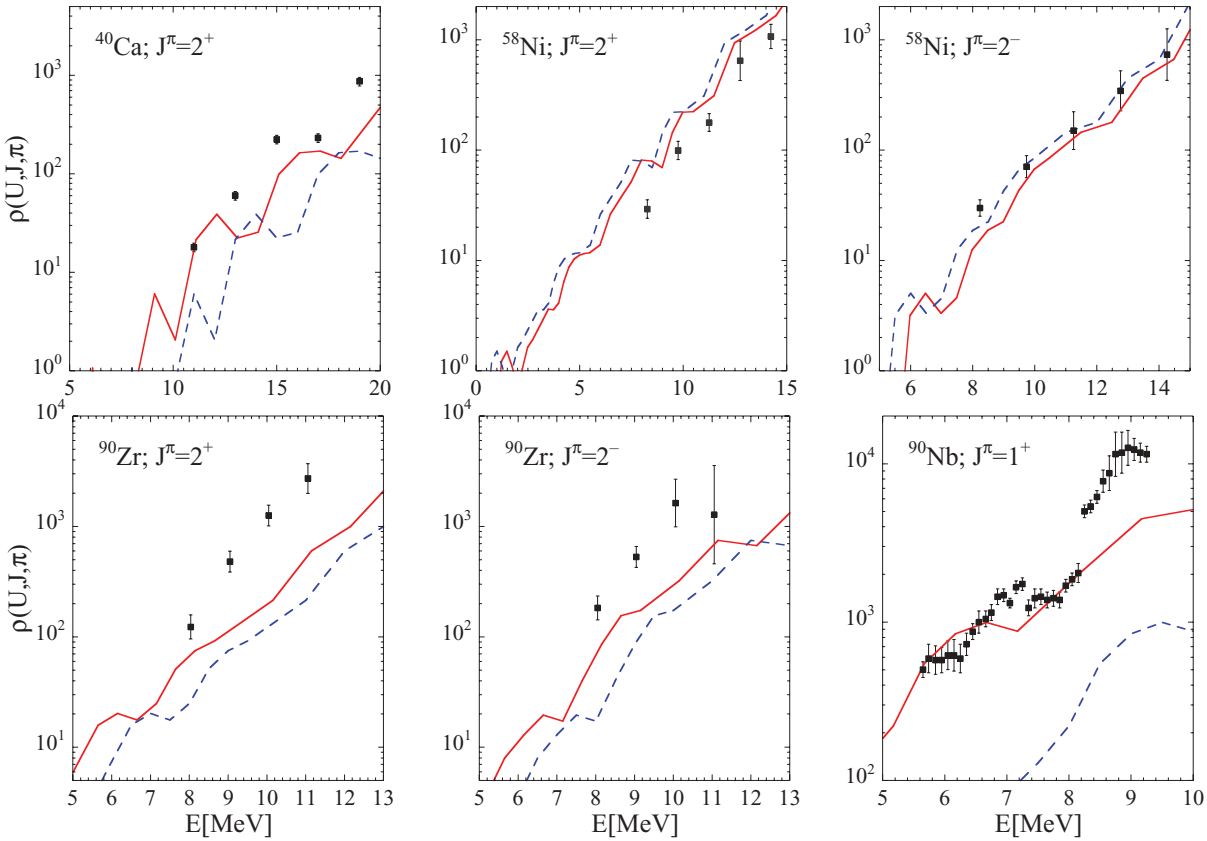

FIG. 10. (Color online) Comparison between theoretical and experimental NLDs for given spin and parity in ^{40}Ca, ^{58}Ni, ^{90}Zr, and ^{90}Nb. The experimental data (full squares) are taken from Ref. [26] for ^{40}Ca and from Ref. [27] for ^{58}Ni, ^{90}Zr, and ^{90}Nb. The blue dashed lines correspond to the raw NLDs and the full red lines to the normalized ones.

When phenomenological NLDs are used for nuclear physics applications, such as nuclear data evaluation or for accurate and reliable estimations of reaction cross sections, one often plays with the few parameters on which phenomenological expressions rely. Although our predictions are provided in a table format, it is possible to renormalize them both on the experimental level scheme at low energy and the neutron resonance spacings at $U = S_n$ in a way similar to what is usually done with analytical formulas. More precisely, the renormalized level density can be obtained through the expression

$$\rho(U, J, P)_{\text{renorm}} = e^{\alpha\sqrt{(U-\delta)}}\ \rho(U-\delta, J, P), \qquad (8)$$

where the energy shift δ is essentially extracted from the analysis of the cumulative number of levels and α from the experimental s-wave neutron spacing. With such a renormalization, the experimental low-lying states and the D_0 values can be reproduced reasonably well as discussed in detail in Ref. [22]. Equation (8) has been used to fit the 289 nuclides for which both an experimental s-wave spacing (D_0) and a discrete level sequence exist. The corresponding δ and α values for these nuclei are shown graphically in Fig. 8 and compared with the same values obtained using our previous model (see Fig. 8 of Ref. [2]). As can be seen, the α and δ parameters show no systematic trend or A dependence, and more particularly no correlation with shell closures. A significant reduction of the normalization factors appears in the actinide region, essentially due to a better description of moments of inertia. For an additional 846 nuclides, only the experimental discrete level scheme with at least 10 levels are known. For those nuclei, only the δ shift is used to reproduce at best the low-lying levels. Sets of δ and α parameters have therefore also been tabulated using the approach of Ref. [22].

We compare in Fig. 9 our predictions with the experimental data extracted by the Oslo group [23,25] for a significant set of nuclei covering quite a wide range of masses. As already mentioned in Ref. [2], the experimental determination is, however, model dependent since a normalization procedure is followed by the Oslo group. The experimental points are indeed normalized to the so-called experimental total NLD at $U = S_n$ deduced from the measured s-neutron resonance spacing on the basis of a BSFG-type formula (see the corresponding points shown as full triangles in Fig. 9). A similar procedure must be followed on the basis of our combinatorial model, determining for each nucleus a value α such that

$$\rho_{\text{th}}(S_n) \times \exp(\alpha\sqrt{S_n}) = \rho_{\text{Oslo}}(S_n), \qquad (9)$$

and then plotting the normalized theoretical level densities (see Ref. [22] for more details). As can be observed, the

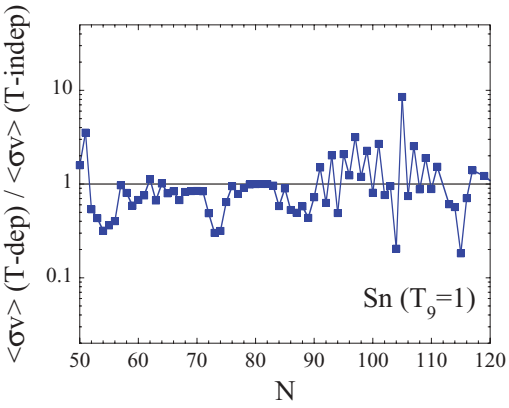

FIG. 11. (Color online) Ratio of Maxwellian-averaged (n, γ) rates obtained with the current NLDs and those of Ref. [2] for tin isotopes for a stellar temperature of $T = 10^9$ K.

combinatorial NLD (thick line in Fig. 9) agrees globally quite well with the so-called experimental values below S_n.

Our predictions are also compared in Fig. 10 with the spin- and parity-dependent level density data extracted from Refs. [26,27]. In this figure, the raw NLDs (blue dotted line) as well as the normalized ones (full red line) are plotted. Note that the normalizations have not been done to fit these experimental data but are those corresponding to the fit to low-lying experimental discrete levels and/or D_0. The agreement is not perfect but both the experimental fluctuations and orders of magnitude are fairly well reproduced by the normalized NLD.

To further compare the present NLDs with those of Ref. [2], we plot in Fig. 11 the ratio of the Maxwellian-averaged (n, γ) rates $\langle \sigma v \rangle$ at the stellar temperature of $T = 10^9$ K for Sn isotopes obtained with the current and previous NLD. The radiative capture rate at such a temperature essentially reflects the cross section around hundred keV incident neutron energy.

At such energies, the radiative capture cross section is known to be sensitive to the NLD below the neutron threshold. As can be seen, the temperature-dependent NLDs provide

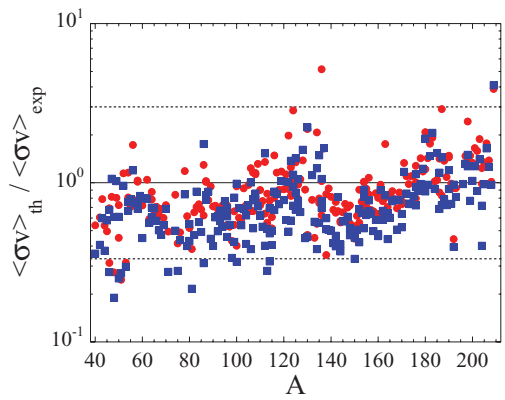

FIG. 12. (Color online) Ratio of TALYS Maxwellian-averaged (n, γ) rates $\langle \sigma v \rangle_{\rm th}$ with experimental values [28] at $T = 3 \times 10^8$ K. The blue squares correspond to the current normalized NLDs and the red dots to those of Ref. [2].

results rather similar to the previous ones though for a few exotic cases deviations by a factor up to 10 can be observed.

Comparisons of the Maxwellian-averaged (n, γ) rates $\langle \sigma v \rangle$ at $T = 3 \times 10^8$ K with experimental data for some 219 nuclei heavier than ^{40}Ca included in the compilation of Bao *et al.* [28] are also shown in Fig. 12 using either the normalized NLDs of our previous model or the current ones. The calculations agree with experimental data roughly within a factor of 2 for both models. Note that additional uncertainties stemming in particular from γ-ray strength functions also affect the predictions. In the present case, the microscopic γ-ray strength functions from Ref. [29] have been used. The corresponding rms deviation [based on a relation identical to Eq. (7)] for the 219 nuclei is $f_{\rm rms} = 1.60$ using the old NLDs and 1.80 with the present ones. This difference is directly correlated to the difference between the corresponding $f_{\rm rms} = 2.3$ and 2.7 obtained with respect to the experimental D_0 values (see Fig. 5 for the present NLDs).

V. CONCLUSIONS AND PROSPECTS

New developments have been brought to our combinatorial method in order to determine on more solid microscopic grounds NLDs and to be able to calculate them for nearly 8500 nuclei. The idea behind this update consists in trying to reduce the amount of phenomenology necessary to determine microscopic level densities usable for application. For this purpose, the D1M Gogny interaction has been used instead of the previously employed Skyrme force to determine the nuclear structure information out of which the NLDs are built. This choice has been made since the Gogny interaction has shown its ability to predict quite well low-energy quadrupole collective levels, both rotational and vibrational, thus enabling us to believe in an improvement of the predictive power of our calculations. Beyond that, we have also implemented a temperature-dependent treatment of the nuclear properties which provides us with a way to deal with the modifications of the structure properties with increasing excitation energies within a more solid physical framework than before. In particular, the use of a microscopic moment of inertia to construct rotational bands in deformed nuclei which evolves with increasing energy enables us to improve the low-energy level descriptions for well-deformed nuclei such as in the rare earth or in the actinide region. The newly derived NLDs are shown to provide fairly good results when compared with experimental data up to the neutron separation energy. Still several problems remain to be investigated, such as the treatment of the coupling between particle-hole and vibrational excited states or the control of the smoothing function enabling the suppression of the discontinuities between spherical and deformed NLDs. This smoothing function still remains the weakest point of the current formalism. Further investigation is required to be able to suppress such an arbitrary function. Other possible improvements concern the microscopic determination of octupole (and possibly hexadecapole) vibrational level energies for which a phenomenological expression is still employed.

[1] H. A. Bethe, Phys. Rev. **50**, 332 (1936).
[2] S. Goriely, S. Hilaire, and A. J. Koning, Phys. Rev. C **78**, 064307 (2008).
[3] S. Hilaire and S. Goriely, Nucl. Phys. A **779**, 63 (2006).
[4] S. Goko *et al.*, Phys. Rev. Lett. **96**, 192501 (2006).
[5] S. Hilaire, J. P. Delaroche, and M. Girod, Eur. Phys. J. A **12**, 169 (2001).
[6] T. Døssing and A. S. Jensen, Nucl. Phys. A **222**, 493 (1974).
[7] G. Hansen and A. S. Jensen, Nucl. Phys. A **406**, 236 (1983).
[8] S. Goriely, M. Samyn, and J. M. Pearson, Phys. Rev. C **75**, 064312 (2007).
[9] G. Audi, A. H. Wapstra, and C. Thibault, Nucl. Phys. A **729**, 337 (2003).
[10] G.F. Bertsch, M. Girod, S. Hilaire, J. P. Delaroche, H. Goutte, and S. Peru, Phys. Rev. Lett. **99**, 032502 (2007).
[11] J. P. Delaroche *et al.*, Phys. Rev. C **81**, 014303 (2010).
[12] J. F. Berger, M. Girod, D. Gogny, Comput. Phys. Commun. **63**, 365 (1991).
[13] S. Hilaire and M. Girod, Eur. Phys. J. A **33**, 237 (2007).
[14] S. Goriely, S. Hilaire, M. Girod, and S. Péru, Phys. Rev. Lett. **102**, 242501 (2009).
[15] S. Péru and H. Goutte, Phys. Rev. C **77**, 044313 (2008).
[16] S. Peru, G. Gosselin, M. Martini, M. Dupuis, S. Hilaire, and J. C. Devaux, Phys. Rev. C **83**, 014314 (2011).
[17] V. Martin, J. L. Egido, and L. M. Robledo, Phys. Rev. C **68**, 034327 (2003).
[18] P. Demetriou and S. Goriely, Nucl. Phys. A **695**, 95 (2001).
[19] S. Goriely, in *Journal of Nuclear Science and Technology: Proceedings of the International Conference on Nuclear Data for Science and Technology, October 7-12, 2001, Supplement 2*, edited by K. Shibata (Atomic Energy Society of Japan, Tokyo, 2002), p. 536.
[20] R. Capote *et al.*, Nucl. Data Sheets **110**, 3107 (2009).
[21] A. Bürger *et al.*, Phys. Rev. C **85**, 064328 (2012).
[22] A. J. Koning, S. Hilaire, and S. Goriely, Nucl. Phys. A **810**, 13 (2008).
[23] A. Voinov, M. Guttormsen, E. Melby, J. Rekstad, A. Schiller, and S. Siem, Phys. Rev. C **63**, 044313 (2001).
[24] S. Siem, M. Guttormsen, K. Ingeberg, E. Melby, J. Rekstad, A. Schiller, and A. Voinov, Phys. Rev. C **65**, 044318 (2002).
[25] M. Guttormsen, A. Bagheri, R. Chankova, J. Rekstad, S. Siem, A. Schiller, and A. Voinov, Phys. Rev. C **68**, 064306 (2003).
[26] I. Usman *et al.*, Phys. Rev. C **84**, 054322 (2011).
[27] Y. Kalmykov, C. Ozen, K. Langanke, G. Martinez-Pinedo, P. von Neumann-Cosel, and A. Richter, Phys. Rev. Lett. **99**, 202502 (2007).
[28] Z. Y. Bao, H. Beer, F. Käppeler *et al.*, At. Data Nucl. Data Tables **75**, 1 (2000).
[29] S. Goriely, E. Khan, and M. Samyn, Nucl. Phys. A **739**, 331 (2004).